Journal of the Mechanics and Physics of Solids 112 (2018) 209–224

Contents lists available at ScienceDirect

Journal of the Mechanics and Physics of Solids

journal homepage: www.elsevier.com/locate/jmps

A continuum mechanics constitutive framework for transverse isotropic soft tissues

D. Garcia-Gonzalez[a,b,*], A. Jérusalem[a], S. Garzon-Hernandez[b], R. Zaera[b], A. Arias[b]

[a] Department of Engineering Science, University of Oxford, Parks Road, Oxford OX1 3PJ, UK
[b] Department of Continuum Mechanics and Structural Analysis, University Carlos III of Madrid, Avda. de la Universidad 30, 28911 Leganés, Madrid, Spain

ARTICLE INFO

Article history:
Received 8 June 2017
Revised 31 October 2017
Accepted 2 December 2017
Available online 5 December 2017

Keywords:
Soft tissues
Strain rate dependence
Temperature dependence
White matter
Skin

ABSTRACT

In this work, a continuum constitutive framework for the mechanical modelling of soft tissues that incorporates strain rate and temperature dependencies as well as the transverse isotropy arising from fibres embedded into a soft matrix is developed. The constitutive formulation is based on a Helmholtz free energy function decoupled into the contribution of a viscous-hyperelastic matrix and the contribution of fibres introducing dispersion dependent transverse isotropy. The proposed framework considers finite deformation kinematics, is thermodynamically consistent and allows for the particularisation of the energy potentials and flow equations of each constitutive branch. In this regard, the approach developed herein provides the basis on which specific constitutive models can be potentially formulated for a wide variety of soft tissues. To illustrate this versatility, the constitutive framework is particularised here for animal and human white matter and skin, for which constitutive models are provided. In both cases, different energy functions are considered: Neo-Hookean, Gent and Ogden. Finally, the ability of the approach at capturing the experimental behaviour of the two soft tissues is confirmed.

© 2017 The Authors. Published by Elsevier Ltd.
This is an open access article under the CC BY-NC-ND license.
(http://creativecommons.org/licenses/by-nc-nd/4.0/)

1. Introduction

A wide variety of materials combines viscous behaviours with transverse isotropy. Examples of these are soft tissues in humans, animals or plants (Zulliger et al., 2004; Gasser et al., 2006; Wang et al., 2014). The mechanical behaviour exhibited by these soft tissues is known to involve complex phenomena such as large deformation and nonlinear response. These features of the mechanical behaviour of soft tissues can be suitably modelled by using hyperelastic theories (Fung, 1981). Moreover, while some authors assume isotropy for their modelling, these biological tissues are commonly embedded with bundles of fibres that present a preferred direction (Murphy, 2013). The presence of these fibres into the tissue generally results in a stiffer response in their preferred direction, also identified as transverse isotropic behaviour (Fung, 1981; Cowin and Humphrey, 2001; Guo et al., 2007). Overall, the incorporation of this directional preference in soft tissues has be-

* Corresponding author at: Department of Engineering Science, University of Oxford, Parks Road, Oxford OX1 3PJ, UK.
E-mail addresses: daniel.garciagonzalez@eng.ox.ac.uk (D. Garcia-Gonzalez), antoine.jerusalem@eng.ox.ac.uk (A. Jérusalem), aariash@ing.uc3m.es (A. Arias).

https://doi.org/10.1016/j.jmps.2017.12.001
0022-5096/© 2017 The Authors. Published by Elsevier Ltd. This is an open access article under the CC BY-NC-ND license.
(http://creativecommons.org/licenses/by-nc-nd/4.0/)

come an essential step to develop reliable mathematical models able to predict the mechanical behaviour of these materials (Murphy, 2013).

A considerable effort has been made in order to experimentally characterise soft tissues. In this regard, experimental work has been carried out on different human and animal tissues embedded with collagen fibres: arteries (Arroyave et al., 2015), soft connective tissue such as skin or tendons (Annaidh et al., 2010; Carniel and Fancello, 2017), muscles (Mohammadkhah et al., 2016) or myocardium in the heart (Humphrey et al., 1990; Murphy, 2013), among others. Another relevant experimental work is the white matter of the brain, where the transverse isotropic behaviour arises from the alignment of the bundles of axons (Prange and Margulies, 2002).

In parallel to these efforts, several authors have modelled biological soft materials by defining their overall mechanical response as the sum of matrix and fibres contributions. Human arteries were studied by Gasser et al. (2006) with the development of a continuum framework accounting for the dispersion of the collagen fibre orientation through a hyperelastic free energy function that also encompassed the anisotropic elastic properties. Skin can be modelled following the same assumptions. It consists of collagen fibres embedded in a ground substance, thus presenting a transversely isotropic nonlinear behaviour (Valero et al., 2015). The tendons are another example of structures characterized by axially oriented bundles of collagen fibres embedded into a ground substance. This prevalent unidimensional fibre orientation is responsible for a greater stiffness and resistance in the axial direction (Maurel et al., 1997; Natali et al., 2005). Natali et al. (2005) formulated an anisotropic elastic constitutive model where a main free energy function was defined as the sum of an isotropic matrix contribution and an anisotropic contribution due to the fibres. Moreover, Velardi et al. (2006) used a transversely isotropic hyperelastic model originally proposed by Meaney (2003) to study the mechanics of the brain under uniaxial tensile tests. Chatelin et al. (2012) proposed a visco-hyperelastic model which takes into account the rate dependency and anisotropy arising from the axonal orientation. More recently, Labus and Puttlitz (2016) developed an anisotropic hyperelastic constitutive model for white matter based on a strain energy density function that also incorporates the anisotropic contribution of the axons.

The dependence of the mechanical behaviour of soft tissues on strain rate and temperature has also been the subject of many research programmes. Pietsch et al. (2014) carried out compression tests at multiple strain rates in both transverse and longitudinal directions using porcine muscle specimens. A stiffer response with higher strain rate was observed. Similarly, Clemmer et al. (2010) investigated the structure of collagen fibril by testing patellar tendon samples from rabbits at different strain rates. Again, an increase in stiffness with strain rate was observed. Similar results were observed by Ng et al. (2004) for chicken tendons. Kulkarni et al. (2016) proposed a transversely isotropic visco-hyperelastic constitutive model for soft tissues in order to account for strain rate effects. In this model, a viscous potential was introduced to describe the rate dependent short-term memory effects. Experiments conducted by Zhou et al. (2010) confirmed a rate-induced hardening for skin, along with a softening response with temperature. Liu et al. (2016) have recently demonstrated a temperature dependence in the brain mechanical properties.

To the authors' knowledge, there is no constitutive model available in the literature that accounts simultaneously for strain rate sensitivity, temperature dependency and anisotropy due to fibres for transversely isotropic soft tissues, in a thermodynamically consistent fashion. In this work, a continuum framework for soft tissues embedded with fibres of different natures is developed. The formulation is based on a Helmholtz free energy function additively decoupled into a viscous-hyperelastic contribution associated with the response of the matrix, which is assumed isotropic; and an anisotropic contribution associated with the response of the fibres, as suggested by Holzapfel et al. (2000). The constitutive framework is applied to white matter of the brain and skin in order to illustrate its versatility. In addition, a methodology based on imaging techniques to incorporate structural information (regarding fibre orientation and dispersion) to the proposed model is presented. For these soft tissues, three different commonly used energy functions are considered in this work: Neo-Hookean (Rivlin, 1948), Gent (Gent, 1996) and Ogden (Ogden, 1972). The identification process of the model parameters depending on each energy function is carried out by applying an optimisation process for each soft tissue. For both soft tissues, a good correlation between experimental data available in the literature and model predictions is found. More generally, this constitutive framework can be used to model specific soft tissues with strain rate and temperature dependencies through the selection of the free energy functions and flow equations of each constitutive branch.

Section 2 details the proposed continuum mechanics framework. Its particularisation to white matter and skin is then described in Sections 3 and 4, and the corresponding results and discussion in Section 5. Section 6 finally concludes this work.

2. Continuum mechanics framework

The proposed continuum mechanics framework is presented here, including the description of the rheological scheme, the finite deformation kinematics, the continuum representation of distributed fibre orientation and the assumptions adopted for the Helmholtz free energy function.

2.1. Rheological model

The rheological model is composed of three constitutive branches: the viscous (V) and the purely elastic (E) branches associated to the matrix behaviour; and the fibres behaviour branch (F), see Fig. 1. Note that the viscous contribution is

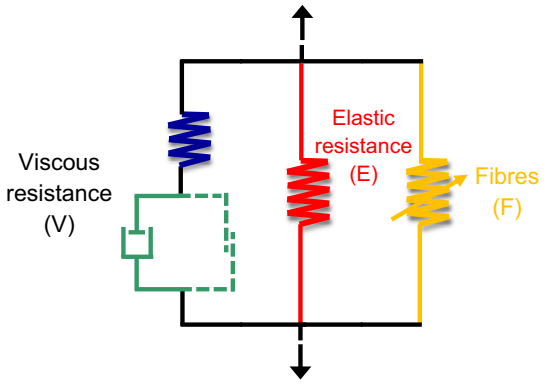

Fig. 1. General rheological scheme.

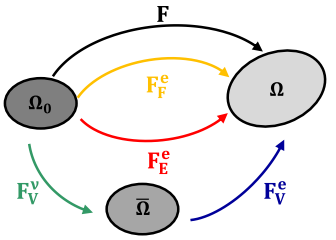

Fig. 2. Kinematics of the framework.

governed by a yield function if the friction element shown in dash lines is present; and it is permanently active otherwise. This model is largely motivated by general observations of the deformation mechanisms of anisotropic hyperelastic soft tissues.

The mechanical response of a variety of transversely isotropic soft tissues has been modelled by many authors by considering the total stress response of the material as the sum of the stress contribution due to fibres embedded in an isotropic matrix, and the one of the matrix itself (Gasser et al., 2006; Kulkarni et al., 2016). Most of the subsequently developed models that follow this assumption describe the matrix response under quasi-static conditions as purely hyperelastic (Chatelin et al., 2012; Labus and Puttlitz, 2016). In this regard, if no strain rate dependency is considered, the matrix behaviour can be described by only defining the hyperelastic spring of the purely elastic branch. As these materials can also exhibit strain rate dependency, the matrix behaviour can instead be captured by being defined as a combination of elastic and viscous responses, the latter being introduced to this effect. The fibres can be modelled with a direction dependent spring which introduces the anisotropy due to fibre orientation.

According to the description of the rheological model (see Fig. 1), the total stress of the transversely isotropic material is postulated as a combination of the stress contributions of each phase:

$$\boldsymbol{\sigma} = \boldsymbol{\sigma}_{\mathbf{M}} + \boldsymbol{\sigma}_{\mathbf{F}} \tag{1}$$

where $\boldsymbol{\sigma}_{\mathbf{M}}$ and $\boldsymbol{\sigma}_{\mathbf{F}}$ are the Cauchy stress contributions of the matrix and the fibres, respectively. The total stress due to the matrix response is obtained as the sum of both viscous and elastic resistances, $\boldsymbol{\sigma}_{\mathbf{M}} = \boldsymbol{\sigma}_{\mathbf{V}} + \boldsymbol{\sigma}_{\mathbf{E}}$.

2.2. Kinematics framework

The finite deformation kinematics is defined by three configurations described next, see Fig. 2. An infinitesimal line element in the reference configuration Ω_0 can be mapped to the current configuration Ω through the total deformation gradient $\mathbf{F}$. Note that the deformation gradient is the same for all the constitutive branches. Thus, $\mathbf{F} = \mathbf{F}_{\mathbf{V}} = \mathbf{F}_{\mathbf{E}} = \mathbf{F}_{\mathbf{F}}$ where $\mathbf{F}_{\mathbf{V}}$ refers to the viscous resistance, $\mathbf{F}_{\mathbf{E}}$ to the purely elastic resistance, and $\mathbf{F}_{\mathbf{F}}$ to the fibres resistance. While the latter two resistances are defined as purely elastic, $\mathbf{F}_{\mathbf{E}}^{\mathbf{e}}$ and $\mathbf{F}_{\mathbf{F}}^{\mathbf{e}}$, respectively, the viscous resistance contribution is decomposed into an elastic $\mathbf{F}_{\mathbf{V}}^{\mathbf{e}}$ and a viscous part $\mathbf{F}_{\mathbf{V}}^{\mathbf{v}}$. Following a multiplicative decomposition of the viscous resistance, an additional intermediate configuration, designated as the relaxed configuration $\bar{\Omega}$, is defined to account for the viscous effects. The following expression for the total deformation gradient is thus obtained:

$$\mathbf{F} = \mathbf{F}_{\mathbf{V}}^{\mathbf{e}}\mathbf{F}_{\mathbf{V}}^{\mathbf{v}} = \mathbf{F}_{\mathbf{E}}^{\mathbf{e}} = \mathbf{F}_{\mathbf{F}}^{\mathbf{e}} \tag{2}$$

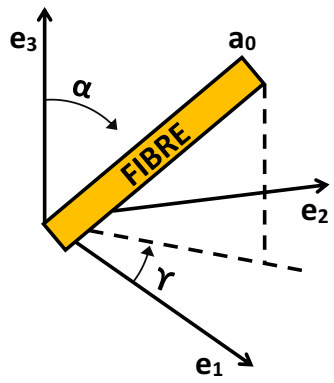

Fig. 3. Characterisation of the unit fibre orientation vector $\mathbf{a_o}$ by means of spherical coordinates.

The velocity gradient $\mathbf{l}$ can be written in terms of the different kinematics of the constitutive branches as:

$$\mathbf{l} = \dot{\mathbf{F}}\mathbf{F}^{-1} = \mathbf{l}_{\mathbf{V}}^{\mathbf{e}} + \mathbf{F}_{\mathbf{V}}^{\mathbf{e}}\bar{\mathbf{L}}_{\mathbf{V}}^{\boldsymbol{\nu}}\mathbf{F}_{\mathbf{V}}^{-\mathbf{e}} \tag{3.1}$$

$$\mathbf{l} = \mathbf{l}_{\mathbf{E}}^{\mathbf{e}} = \mathbf{l}_{\mathbf{F}}^{\mathbf{e}} \tag{3.2}$$

where $\mathbf{l}_{\mathbf{V}}^{\mathbf{e}} = \dot{\mathbf{F}}_{\mathbf{V}}^{\mathbf{e}}\mathbf{F}_{\mathbf{V}}^{-\mathbf{e}}$, $\mathbf{l}_{\mathbf{E}}^{\mathbf{e}} = \dot{\mathbf{F}}_{\mathbf{E}}^{\mathbf{e}}\mathbf{F}_{\mathbf{E}}^{-\mathbf{e}}$ and $\mathbf{l}_{\mathbf{F}}^{\mathbf{e}} = \dot{\mathbf{F}}_{\mathbf{F}}^{\mathbf{e}}\mathbf{F}_{\mathbf{F}}^{-\mathbf{e}}$ are respectively the elastic parts of the viscous, elastic and fibre velocity gradient expressed in Ω. $\bar{\mathbf{L}}_{\mathbf{V}}^{\boldsymbol{\nu}} = \dot{\mathbf{F}}_{\mathbf{V}}^{\boldsymbol{\nu}}\mathbf{F}_{\mathbf{V}}^{-\boldsymbol{\nu}}$ is the viscous part of the viscous velocity gradient expressed in $\bar{\Omega}$.

2.3. Continuum representation of the distributed fibre orientation

This section describes a methodology defining a scalar parameter that represents the average deformation along the fibres direction (Gasser et al., 2006). In the following sections, the representation of distributed fibre orientation is particularised for different transversely isotropic materials. The orientation of the fibres and their distribution is introduced in a continuum sense through a symmetric structure tensor $\mathbf{A_o}$ depending on the orientation density function $\rho(\mathbf{a_o})$ which characterises the fibre distribution (Advani and Tucker, 1987; Gasser et al., 2006):

$$\mathbf{A_o} = \frac{1}{4\pi}\int_{\mathrm{W}} \rho(\mathbf{a_o})\mathbf{a_o}\otimes\mathbf{a_o}\mathrm{dW} \tag{4}$$

where W is a unit sphere and $\mathbf{a_o}$ an arbitrary unit fibre orientation vector defined in Ω_o, that can be expressed by using two spherical coordinates $\alpha\in[0,\pi]$ and $\gamma\in[0,2\pi]$, see Fig. 3:

$$\mathbf{a_o}(\alpha,\gamma) = \sin\alpha\cos\gamma\,\mathbf{e}_1 + \sin\alpha\sin\gamma\,\mathbf{e}_2 + \cos\alpha\,\mathbf{e}_3 \tag{5}$$

where $\mathbf{e}_{i=1,2,3}$ denote the Cartesian coordinate basis.

The compact form of the structure tensor of orientation can be written as:

$$\mathbf{A_o} = \mathrm{A_{oij}}\mathbf{e_i}\otimes\mathbf{e_j} \tag{6}$$

where the coefficients $\mathrm{A_{oij}} = \mathrm{A_{oji}}$ (symmetric tensor) are defined as proposed by Gasser et al. (2006):

$$\left.\begin{aligned}
\mathrm{A_{o11}} &= \frac{1}{4\pi}\int_0^{2\pi}\int_0^{\pi}\rho(\alpha,\gamma)\sin^3\alpha\cos^2\gamma\,\mathrm{d}\alpha\mathrm{d}\gamma\\
\mathrm{A_{o22}} &= \frac{1}{4\pi}\int_0^{2\pi}\int_0^{\pi}\rho(\alpha,\gamma)\sin^3\alpha\sin^2\gamma\;\mathrm{d}\alpha\mathrm{d}\gamma\\
\mathrm{A_{o33}} &= \frac{1}{4\pi}\int_0^{2\pi}\int_0^{\pi}\rho(\alpha,\gamma)\cos^2\alpha\sin\alpha\mathrm{d}\alpha\mathrm{d}\gamma\\
\mathrm{A_{o12}} &= \frac{1}{4\pi}\int_0^{2\pi}\int_0^{\pi}\rho(\alpha,\gamma)\sin^3\alpha\sin\gamma\cos\gamma\mathrm{d}\alpha\mathrm{d}\gamma\\
\mathrm{A_{o23}} &= \frac{1}{4\pi}\int_0^{2\pi}\int_0^{\pi}\rho(\alpha,\gamma)\sin^2\alpha\cos\alpha\sin\gamma\mathrm{d}\alpha\mathrm{d}\gamma\\
\mathrm{A_{o13}} &= \frac{1}{4\pi}\int_0^{2\pi}\int_0^{\pi}\rho(\alpha,\gamma)\sin^2\alpha\cos\alpha\cos\gamma\mathrm{d}\alpha\mathrm{d}\gamma
\end{aligned}\right\} \tag{7}$$

The average stretch of the fibres $\bar{\lambda}_{\mathrm{F}}$ can then be defined as:

$$\bar{\lambda}_{\mathrm{F}} = \sqrt{\mathrm{I_{4F}}} \tag{8}$$

where I_{4F} is the fourth strain invariant that depends on $\mathbf{A_o}$ and on the elastic right Cauchy-Green deformation tensor of the fibres $\mathbf{C_F^e}$ through:

$$I_{4F} = \mathrm{tr}\left(\mathbf{A_o C_F^e}\right) \tag{9}$$

In soft tissues, the structure tensor is commonly given in a compact form considering transversely isotropic distribution of the fibres. This is the case of brain white matter in which the distribution of axons can be extracted from experimental techniques, see following sections.

2.4. Derivation of the stress tensors from the Helmholtz free energy function

The Helmholtz free energy function Ψ_o per unit volume in Ω_o is defined here as depending on the elastic right Cauchy–Green deformation tensors $\mathbf{C_V^e} = \mathbf{F_V^{eT}F_V^e}$, $\mathbf{C_E^e} = \mathbf{F_E^{eT}F_E^e}$ and $\mathbf{C_F^e} = \mathbf{F_F^{eT}F_F^e}$, temperature θ and structure tensor $\mathbf{A_o}$. In addition, it is decoupled into its matrix (Ψ_{oM}) and fibres (Ψ_{oF}) contributions:

$$\Psi_o = \Psi_{oM}\left(\mathbf{C_V^e}, \mathbf{C_E^e}, \theta\right) + \Psi_{oF}\left(\mathbf{C_F^e}, \mathbf{A_o}, \theta\right) \tag{10}$$

Furthermore, the matrix part can be assumed to be the combination of the viscous (Ψ_{oM}^{V}) and elastic (Ψ_{oM}^{E}) resistances:

$$\Psi_{oM} = \Psi_{oM}^{V}\left(\mathbf{C_V^e}, \theta\right) + \Psi_{oM}^{E}\left(\mathbf{C_E^e}, \theta\right) \tag{11}$$

Note that the consideration of the viscous contribution to the energy function of the matrix results in an isotropic viscous response.

Starting from the first and second Thermodynamics Principles and considering the expression of the Helmholtz free energy assumed herein, the following expression for the Clausius–Duhem inequality is obtained:

$$-\dot{\Psi}_o - \dot{\theta}\eta_o + \mathbf{M_{oV}} : \mathbf{D_V^v} + \mathbf{S_{oV}} : \mathbf{F^T D_V^e F} + \mathbf{S_{oE}} : \mathbf{F^T D_E^e F} + \mathbf{S_{oF}} : \mathbf{F^T D_F^e F} - \frac{1}{\theta}\mathbf{q}\nabla_x\theta \geq 0 \tag{12}$$

where $\mathbf{S_{oV}}$, $\mathbf{S_{oE}}$ and $\mathbf{S_{oF}}$ are the second Piola-Kirchhoff stresses in Ω_o of the viscous, elastic and fibre resistances; $\mathbf{M_{oV}} = \mathbf{F^T F S_{oV}}$, is the Mandel stresses in Ω_o of the viscous resistance; $\mathbf{D_V^e}$, $\mathbf{D_E^e}$ and $\mathbf{D_F^e}$ are the symmetric parts of the velocity gradient tensors in Ω_o of the viscous, elastic and fibre resistances; $\mathbf{D_V^v}$ is the symmetric part of the viscous velocity gradient tensor in Ω_o; η_o is the specific entropy per unit volume in Ω_o; and $\mathbf{q} = -k\nabla_x\theta$ is the heat flux per unit volume in Ω_o, with k being the thermal conductivity. $\dot{\Psi}_o$ can then be derived as

$$\dot{\Psi}_o = \frac{\partial \Psi_o}{\partial \mathbf{C_V^e}} : \dot{\mathbf{C}}_\mathbf{V}^\mathbf{e} + \frac{\partial \Psi_o}{\partial \mathbf{C_E^e}} : \dot{\mathbf{C}}_\mathbf{E}^\mathbf{e} + \frac{\partial \Psi_o}{\partial \mathbf{C_F^e}} : \dot{\mathbf{C}}_\mathbf{F}^\mathbf{e} + \frac{\partial \Psi_o}{\partial \theta}\dot{\theta} \tag{13}$$

Therefore, by substituting Eq. (13) into Eq. (12), the Clausius–Duhem inequality can be rewritten as:

$$\left(\mathbf{F_V^v S_{oV} F_V^{vT}} - 2\frac{\partial \Psi_o}{\partial \mathbf{C_V^e}}\right) : \mathbf{F_V^{eT} D_V^e F_V^e} + \left(\mathbf{S_{oE}} - 2\frac{\partial \Psi_o}{\partial \mathbf{C_E^e}}\right) : \mathbf{F_E^{eT} D_E^e F_E^e} + \left(\mathbf{S_{oE}} - 2\frac{\partial \Psi_o}{\partial \mathbf{C_F^e}}\right) : \mathbf{F_F^{eT} D_F^e F_F^e} + \mathbf{M_{oV}} : \mathbf{D_V^v}$$
$$+ \left(-\frac{\partial \Psi_o}{\partial \theta} - \eta_o\right)\dot{\theta} - \frac{1}{\theta}\mathbf{q}\nabla_x\theta \geq 0 \tag{14}$$

From this equation, the second Piola-Kirchhoff stress associated to each constitutive branch and the specific internal entropy per unit volume can be obtained using the Coleman and Noll method (Coleman and Noll, 1963; Coleman and Gurtin, 1967):

$$\begin{cases} \mathbf{S_{oV}} = \mathbf{F_V^{-v}} 2\dfrac{\partial \Psi_o}{\partial \mathbf{C_V^e}} \mathbf{F_V^{-vT}} & (15.1) \\ \mathbf{S_{oE}} = 2\dfrac{\partial \Psi_o}{\partial \mathbf{C_E^e}} & (15.2) \\ \mathbf{S_{oF}} = 2\dfrac{\partial \Psi_o}{\partial \mathbf{C_F^e}} & (15.3) \\ \eta_o = -\dfrac{\partial \Psi_o}{\partial \theta} & (15.4) \end{cases}$$

It can be demonstrated that the heat conduction term is always positive. Note that for the inelastic dissipation term, the associated flow rule must also satisfy the Clausius-Duhem inequality ($\mathbf{M_{oV}} : \mathbf{D_V^v} \geq 0$).

The continuum mechanics framework presented herein allows for its particularisation to the specific matrix and fibres to be modelled.

3. Particularisation of the energy functions and flow rules

In this work, the versatility of the model is illustrated by defining the framework for two transversely isotropic soft tissues: skin and white matter of the brain. The brain tissue can be divided into grey and white matters. While the grey matter generally exhibits an isotropic mechanical response (Velardi et al., 2006; Pervin and Chen, 2009), the bundles of axons in the white matter induce transverse isotropy. In this work, the mechanical behaviour of the white matter has been modelled as the combination of an isotropic response associated to the glial matrix and an anisotropic response associated to the axonal contribution (Feng et al., 2013; Ning et al., 2006; Velardi et al., 2006). The mechanical response of skin can be understood as the sum of the ground substance contribution (matrix) and the collagen fibres contribution (Valero et al., 2015). The orientation of these collagen fibres is defined by the Langer's lines, within the dermis, that induce a stiffer mechanical resistance to deformation along this direction. The aim of this section is to demonstrate that under the assumptions made in the general framework of this work, it is possible to provide new constitutive models to predict the mechanical behaviour of a wide variety of soft tissues. In order to show the versatility of the model, a set of different free energy functions are defined for brain and skin tissues.

3.1. Particularisation of the isotropic matrix response

The isotropic matrix contribution is defined by the combination of a purely elastic branch with a viscous branch. The purely elastic contribution governs the mechanical response under quasi-static loads whereas the viscous contribution accounts for hardening effects due to strain rate sensitivity (Garcia-Gonzalez et al., 2017a).

3.1.1. Elastic branch

This part of the model has been defined by using a hyperelastic strain energy function. Three different functions have been considered here whose suitability for each soft tissue is presented in the next section: Neo-Hookean energy function, Eq. (16.1) (Rivlin, 1948); Gent energy function, Eq. (16.2) (Gent, 1996); Ogden energy function, Eq. (16.3) (Ogden, 1972).

$$\Psi^{E}_{oM}|_{NH}\left(\mathbf{C}^{e}_{E},\theta\right)=\frac{\mu(\theta)}{2}(I^{*}_{1E}-3)+\frac{1}{2}\kappa(J_{E}-1)^{2} \tag{16.1}$$

$$\Psi^{E}_{oM}|_{G}\left(\mathbf{C}^{e}_{E},\theta\right)=-\frac{\mu(\theta)}{2}j_{m}\ln\left(1-\frac{I^{*}_{1E}-3}{j_{m}}\right)+\frac{1}{2}\kappa(J_{E}-1)^{2} \tag{16.2}$$

$$\Psi^{E}_{oM}|_{O}\left(\mathbf{C}^{e}_{E},\theta\right)=\Psi^{E}_{oM}|_{O}\left(\lambda^{e}_{E1},\lambda^{e}_{E2},\lambda^{e}_{E3},\theta\right)=\frac{\mu(\theta)}{\alpha}\left[\left(\lambda^{e}_{E1}\right)^{\alpha}+\left(\lambda^{e}_{E2}\right)^{\alpha}+\left(\lambda^{e}_{E3}\right)^{\alpha}-3\right]+\frac{1}{2}\kappa(J_{E}-1)^{2} \tag{16.3}$$

where $I^{*}_{1E}=\mathrm{tr}\,\mathbf{C}^{e*}_{E}$ is the isochoric first strain invariant, λ^{e}_{Ei} are the elastic principal stretches of the isochoric part of deformation with $i=1,2,3$ and κ is the bulk modulus. The distortional right Cauchy–Green deformation tensor is defined by $\mathbf{C}^{e*}_{E}=(\mathbf{F}^{e*}_{E})^{T}\mathbf{F}^{e*}_{E}$ where $\mathbf{F}^{e*}_{E}=J_{E}^{-1/3}\mathbf{F}_{E}$, and j_m and α are dimensionless parameters. The shear modulus of the matrix depends on the temperature through $\mu(\theta)=\mu_o+c(\theta-\theta_{ref})$, where c is a material parameter, θ_{ref} is the reference temperature and μ_o is the shear modulus at reference temperature. This linear dependence of brain tissue and skin shear response on temperature is derived from the experimental results obtained by Liu et al. (2016) and Zhou et al. (2010). Note that in the Ogden model, the equivalent shear modulus results from $\mu(\theta)\alpha/2$. In this regard, the physical consistent condition $\mu(\theta)\alpha\geq 0$ must be verified (Ogden et al., 2004). The volumetric term $\frac{1}{2}\kappa(J_{E}-1)^{2}$, although defined in the free energy of the matrix, represents the volumetric response of the overall soft tissue.

The constitutive equation for the network resistance can be derived by using Eq. (15.2) and the stress tensors relation $\boldsymbol{\sigma}_{E}=J_{E}^{-1}\mathbf{F}\mathbf{S}_{oE}\mathbf{F}^{T}$. For the Ogden free energy function, the Eq. (15.2) can be alternatively written in terms of the principal stretches λ^{e}_{Ei} and the principal referential directions $\mathbf{N_i}$ as $\mathbf{S_{oE}}=\sum_{i=1}^{3}\frac{1}{\lambda^{e}_{Ei}}\frac{\partial\Psi_{o}}{\partial\lambda^{e}_{Ei}}\mathbf{N}_{i}\otimes\mathbf{N}_{i}$.

3.1.2. Viscous branch

This part of the model introduces the mechanical dependence on strain rate. As for the elastic branch, three different functions have been considered here whose suitability for each soft tissue is presented in the next section: Neo-Hookean energy function, Eq. (17.1) (Rivlin, 1948); Gent energy function, Eq. (17.2) (Gent, 1996); Ogden energy function, Eq. (17.3) (Ogden, 1972).

$$\Psi^{V}_{oM}|_{NH}\left(\mathbf{C}^{e}_{V}\right)=\frac{\mu_{V}}{2}(I^{e*}_{1V}-3) \tag{17.1}$$

$$\Psi^{V}_{oM}|_{G}\left(\mathbf{C}^{e}_{V}\right)=-\frac{\mu_{V}}{2}j_{V}\ln\left(1-\frac{I^{e*}_{1V}-3}{j_{V}}\right) \tag{17.2}$$

$$\Psi^{V}_{oM}|_{O}\left(\mathbf{C}^{e}_{V}\right)=\Psi^{V}_{oM}|_{O}\left(\lambda^{e}_{V1},\lambda^{e}_{V2},\lambda^{e}_{V3}\right)=\frac{\mu_{V}}{\beta}\left[\left(\lambda^{e}_{V1}\right)^{\beta}+\left(\lambda^{e}_{V2}\right)^{\beta}+\left(\lambda^{e}_{V3}\right)^{\beta}-3\right] \tag{17.3}$$

where μ_V, j_V and β are material parameters. Note that here, $I_{1V}^{e*} = \text{tr}\,\mathbf{C}_\mathbf{V}^{e*}$ and λ_{Vi}^{e} are referred to as the isochoric first strain invariant and the elastic principal stretches (with $i = 1,2,3$) of the viscous resistance (V in Fig. 1). The distortional right Cauchy–Green deformation tensor of the viscous branch is defined by $\mathbf{C}_\mathbf{V}^{e*} = (\mathbf{F}_\mathbf{V}^{e*})^T\mathbf{F}_\mathbf{V}^{e*}$ where $\mathbf{F}_\mathbf{V}^{e*} = J_V^{-1/3}\mathbf{F}_\mathbf{V}^{e}$. Note that the physical consistent condition $\mu_V\beta \geq 0$ must also be verified (Ogden et al., 2004).

The constitutive equation for the network resistance can be derived by using Eq. (15.1) and the stress tensors relation $\boldsymbol{\sigma}_\mathbf{V} = J_E^{-1}\mathbf{F}\mathbf{S}_{\mathbf{oV}}\mathbf{F}^\mathbf{T}$. For the Ogden free energy function, Eq. (15.1) can be alternatively written in terms of the principal stretches λ_{Vi}^{e} and the principal referential directions $\mathbf{N_i}$ as $\mathbf{S}_{\mathbf{oV}} = \mathbf{F}_\mathbf{V}^{-\boldsymbol{\nu}}\left(\sum_{i=1}^{3}\frac{1}{\lambda_{Vi}^{e}}\frac{\partial\Psi_o}{\partial\lambda_{Vi}^{e}}\mathbf{N}_i\otimes\mathbf{N}_i\right)\mathbf{F}_\mathbf{V}^{-\boldsymbol{\nu}T}$.

The viscous part of the deformation gradient is determined by the viscous flow rule. The evolution of this viscous flow is defined as:

$$\bar{\mathbf{L}}_\mathbf{V}^{\boldsymbol{\nu}} = \dot{\mathbf{F}}_\mathbf{V}^{\boldsymbol{\nu}*}\mathbf{F}_\mathbf{V}^{-\boldsymbol{\nu}*} = \dot{\gamma}^{\nu}\bar{\mathbf{N}}^{\mathbf{v}} \tag{18}$$

where $\bar{\mathbf{L}}_\mathbf{V}^{\boldsymbol{\nu}}$ is the viscous component of the velocity gradient in $\bar{\Omega}$, $\dot{\gamma}^{\nu}$ is the viscous multiplier and $\bar{\mathbf{N}}^{\mathbf{v}}$ provides the direction of the viscous flow following:

$$\bar{\mathbf{N}}^{\mathbf{v}} = \frac{\boldsymbol{\sigma}_\mathbf{V}^{\mathbf{dev}}}{\tau_V} \tag{19}$$

where $\boldsymbol{\sigma}_\mathbf{V}^{\mathbf{dev}}$ is the deviatoric part of the Cauchy stress tensor and $\tau_V = \sqrt{\text{tr}(\boldsymbol{\sigma}_\mathbf{V}^{\mathbf{dev}}\boldsymbol{\sigma}_\mathbf{V}^{\mathbf{dev}})}$ is the effective stress driving the viscous flow. The rate equation for viscous flow is given by Bergstrom (2015):

$$\dot{\gamma}^{\nu} = \dot{\gamma}_o^{\nu}\left(\frac{\sqrt{\boldsymbol{\sigma}_\mathbf{V}^{\mathbf{dev}} : \boldsymbol{\sigma}_\mathbf{V}^{\mathbf{dev}}}}{\sqrt{2}\sigma_{VT}}\right)^n \tag{20}$$

where $\dot{\gamma}_o^{\nu}$ is a dimensional scaling constant, and σ_{VT} and n are material properties.

3.2. Particularisation of the anisotropic fibres response

Helmholtz free energy

The free energy associated to the fibres contribution and accounting for the resulting anisotropy can be defined by the free energy function proposed by Gasser et al. (2006):

$$\bar{\Psi}_{oF}^{F}\left(\mathbf{C}_\mathbf{F}^{\mathbf{e}}, \mathbf{A_o}, \theta\right) = \begin{cases} \dfrac{k_1(\theta)}{2k_2}\{\exp[k_2(I_{4F}^{*}-1)^2]-1\} & if\ I_{4F}^{*} \geq 0 \\ 0 & Otherwise \end{cases} \tag{21}$$

where $k_1(\theta) = k_{1o} + c(\theta - \theta_{ref})$ quantifies the increase of stiffness in the fibre direction. k_{1o} is the value of k_1 at the reference temperature θ_{ref}, and c and k_2 are material parameters (c is assumed to be the same as the one of the ground matter, as a first approximation). The isochoric fourth strain invariant $I_{4F}^{*} = \text{tr}(\mathbf{A_o}\mathbf{C}_\mathbf{F}^{e*}) = J_F^{-2/3}I_{4F}$ depends on the distortional right Cauchy–Green deformation tensor $\mathbf{C}_\mathbf{F}^{e*} = (\mathbf{F}_\mathbf{F}^{*})^T\mathbf{F}_\mathbf{F}^{*}$ where $\mathbf{F}_\mathbf{F}^{*} = J_F^{-1/3}\mathbf{F}_\mathbf{F}^{e}$. Note that the fibre anisotropic contribution to the free energy only appears when the fibres are in tension ($I_{4F}^{*} \geq 0$ implies $\bar{\lambda}_F \geq 0$ according to Eq. (8)). Additionally, more complex switch condition can easily be adopted if needed, e.g., Li et al. (2017).

The constitutive equation for the network resistance can be derived by using Eq. (15.3) and the stress tensors relation $\boldsymbol{\sigma}_\mathbf{F} = J_F^{-1}\mathbf{F}\mathbf{S}_{\mathbf{oF}}\mathbf{F}^\mathbf{T}$:

$$\boldsymbol{\sigma}_\mathbf{F} = \begin{cases} \dfrac{2k_1(\theta)}{J_F}(I_{4F}^{*}-1)\exp[k_2(I_{4F}^{*}-1)^2]\text{dev}(\mathbf{F}_\mathbf{F}^{*}\mathbf{A_o}\mathbf{F}_\mathbf{F}^{*T}) & if\ I_{4F}^{*} \geq 0 \\ 0 & Otherwise \end{cases} \tag{22}$$

4. Particularisation of the structure tensor

In this section, a particularisation of the continuum representation of the distributed fibre orientation is presented for: i) axons in the white matter; and ii) collagen fibres in skin.

4.1. Continuum representation of the distributed axonal orientation in the white matter

Many research initiatives on the brain white matter have focussed on the development and use of novel experimental techniques aimed at identifying its underlying axonal structure (Goriely et al., 2015). The main objective of this section is the definition of the structure tensor, Eq. (4), from diffusion tensor imaging (DTI). DTI leverages the use of magnetic resonance imaging (MRI) to measure directional water diffusion in soft tissues predominantly following the fibres paths. The application of DTI to the white matter provides a diffusion tensor from which information on axonal orientation and axonal dispersion within the tissue can be identified for each voxel.

In order to define the particularised structure tensor $\hat{\mathbf{A}}_{\mathbf{o}}$ as a function of a single dispersion parameter ξ and the preferred axonal orientation $\hat{\mathbf{a}}_{\mathbf{o}}$, Gasser et al. (2006) have proposed the following compact form:

$$\hat{\mathbf{A}}_{\mathbf{o}} = \xi \mathbf{I} + (1 - 3\xi)\hat{\mathbf{a}}_{\mathbf{o}} \otimes \hat{\mathbf{a}}_{\mathbf{o}} \tag{23}$$

Significant efforts have recently been made to incorporate the information obtained from DTI into finite element models (Chatelin et al., 2012). This is generally done by mapping a fractional anisotropy (FA) coefficient that represents the *degree of anisotropy* as well as the preferred axon orientation into the finite element mesh. The coefficient FA is defined from the eigenvalues λ_i of the diffusion tensor as proposed by Pierpaoli and Basser (1996):

$$\mathrm{FA} = \frac{\sqrt{3\left[(\lambda_1 - \lambda)^2 + (\lambda_2 - \lambda)^2 + (\lambda_3 - \lambda)^2\right]}}{\sqrt{2\left(\lambda_1^2 + \lambda_2^2 + \lambda_3^2\right)}} \tag{24}$$

where

$$\langle\lambda\rangle = (\lambda_1 + \lambda_2 + \lambda_3)/3 \tag{25}$$

According to the definition of FA, this is a non-dimensional measure that represents the degree of anisotropy in the axon orientation for each voxel volume. This coefficient adopts a value of 0 in the case of an isotropic distribution of the axons and a value of 1 in the case of an ideal co-alignment of the axons. Note that an absence of axons also leads to FA = 0. As a consequence, the use of FA as an anisotropic distribution parameter has often been disputed. While we acknowledge this limitation, we adopt the use of FA as a first approximation of anisotropic distribution.

The definition of the structure tensor presented in Eq. (23) has been previously used by Wright et al. (2013) to incorporate neural tract alignment through DTI and a functional dependence on FA was proposed for the dispersion parameter ξ:

$$\xi = \frac{1}{2}\frac{-6 + 4\mathrm{FA}^2 + 2\sqrt{3\mathrm{FA}^2 - 2\mathrm{FA}^4}}{-9 + 6\mathrm{FA}^2} \tag{26}$$

Therefore, when ξ adopts a value of 1/3, an isotropic distribution of the axons is expected and, in this case, the structure tensor is spherical. When ξ adopts a value of 0, an ideal coalignment of the axons is expected and the structure tensor reduces to $\hat{\mathbf{A}}_{\mathbf{o}} = \hat{\mathbf{a}}_{\mathbf{o}} \otimes \hat{\mathbf{a}}_{\mathbf{o}}$. Thus, the anisotropic behaviour of the white matter due to both axon orientation and axon dispersion can be taken into account in the constitutive modelling through $\hat{\mathbf{A}}_{\mathbf{o}}$ by connecting experiments with modelling. With respect to the preferred axon orientation, an anisotropic unit vector $\hat{\mathbf{a}}_{\mathbf{o}}$ is defined as the mean orientation of the axons in each voxel volume. The direction of the unit vector $\hat{\mathbf{a}}_{\mathbf{o}}$ is given by the eigenvector associated with the maximal eigenvalue of the diffusion tensor (Chatelin et al., 2012).

Giordano and Kleiven (2014) have demonstrated that the white matter stiffness is region-dependent and that there is a direct relation between stiffness and FA whereby the former increases with the latter. The use of the previous definition of the particularised structure tensor $\hat{\mathbf{A}}_{\mathbf{o}}$ in Eqs. (21) and (22), allows us to account for this region dependent stiffness through FA. This approach presents the drastic advantage that the material parameters k_1 and k_2 are the same for the whole white matter, while the anisotropy arises through the experimental knowledge of the FA. This allows for the consideration of not only the anisotropy associated to axon orientation but also for the difference in terms of stiffness depending on regional axon dispersion. Note that the relatively high isotropy of the grey matter (mainly constituted of cell bodies) can equally be modelled by taking a value of FA equal to 0 (Cercignani et al., 2001; Wright et al., 2013). Also, for the ovine white matter, as no DTI was provided only the axonal perfect coalignment case FA = 1 was considered.

4.2. Continuum representation of the distributed orientation of collagen fibres in the skin

Mesoscopically (centimetre scale), skin collagen fibres along Langer's lines can be considered as quasi-perfectly coaligned: $\hat{\mathbf{A}}_{\mathbf{o}} = \hat{\mathbf{a}}_{\mathbf{o}} \otimes \hat{\mathbf{a}}_{\mathbf{o}}$, see also Eq. (23).

5. Analysis and discussion

With the aim of illustrating the versatility of the model, this section presents the predictions of the model for: i) animal (ovine) and human white matter tissues; ii) animal (pig) and human skin tissues. To this end, the model was implemented in MATLAB where the model parameters calibration was carried out by means of optimisation techniques for each soft tissue. A detailed analysis of the energy functions suitability and the optimisation of the model parameters is presented next. The subsequent results and discussion presented in this section are based on the optimal solution found for the mechanical modelling of each tissue studied.

Table 1
Coefficients of determination R^2 for ovine and human white matters for the energy functions considered.

	Coefficient of determination		
	Neo-Hookean	Gent	Ogden
Axon direction (ovine)	0.9920	0.9931	0.9934
Transverse direction (ovine)	0.8177	0.9400	0.9822
Corpus callosum (human)	0.9802	0.9803	0.9807
Corona radiata (human)	0.9098	0.9097	0.9131

Table 2
Coefficients of determination R^2 for pig and human skins for the energy functions considered.

	Coefficient of determination		
	Neo-Hookean	Gent	Ogden
Axon direction (human)	0.9628	0.9641	0.9651
Transverse direction (human)	0.6158	0.9020	0.9302
Mean: strain rate curves (pig)	0.9067	0.9895	0.9826
Mean: temperature curve (pig)	0.9246	0.9822	0.9807

5.1. Analysis of the energy functions and determination of model parameters

This section presents the optimisation procedure used to calibrate the model parameters. To this end, the calibration for each energy function (Neo-Hookean, Gent and Ogden) aims at minimising the following objective function:

$$\mathrm{s} = \sum_{j=1}^{\mathrm{m}} \frac{\sum_{i=1}^{\mathrm{n}} |\mathrm{y}_i - f_i|}{\mathrm{m}} \tag{27}$$

where m is the number of curves of each data collection, f_i are the interpolated values of stress model predictions at experimental strain data, y_i are the experimental stress values and n the number of experimental data points. Two algorithms were employed for this purpose: an unconstrained derivate-free method (*fminseach*, in MATLAB terminology) and a sequential quadratic programming method (*fmincon*, in MATLAB terminology). In addition, the coefficient of determination R^2 was calculated for each energy function and soft tissue considered to evaluate the accuracy (goodness) of fit:

$$R^2 = 1 - \frac{\mathrm{s}^{\mathrm{res}}}{\mathrm{s}^{\mathrm{tot}}} \tag{28}$$

where $\mathrm{s}^{\mathrm{res}} = \sum_{i=1}^{\mathrm{n}} (\mathrm{y}_i - \mathrm{f}_i)^2$ and $\mathrm{s}^{\mathrm{tot}} = \sum_{i=1}^{\mathrm{n}} (\mathrm{y}_i - \bar{\mathrm{y}})^2$, with $\bar{\mathrm{y}}$ being the mean of the experimental data.

This optimisation process was carried out for the animal and human tissues considered. In this regard, different examples collected from literature are analysed and the model parameters are identified and provided for them. The coefficients of determination for each energy function are provided in Table 1 for white matters and in Table 2 for skins. In addition, a section with the parameters of each tissue model is included in the *Appendix A*.

5.2. Discussion

Although some authors have defined the matrix response of transversely isotropic soft tissues with a Neo-Hookean function (Limbert and Middleton, 2004; Kulkarni et al., 2016; Garcia-Gonzalez et al., 2017b), such choice was not found to provide reliable predictions for the tissues and conditions studied herein, while the Gent or Ogden energy functions were shown to perform adequately (see accuracy of the fit for the different models in Tables 1 and 2 by means of R^2). In the following, we discuss in detail the results for both tissues.

5.2.1. White matter

The mechanical behaviour dependence of white matter on applied loading direction, temperature and brain region are incorporated in the proposed constitutive framework. In this section, we focus our discussion on the axonal orientation and corresponding FA.

Animal white matter: axon orientation and temperature dependent properties. Some authors have observed that white matter tissue exhibits a significantly stiffer response when the loading is applied in the axon direction as opposed to the transverse direction (Velardi et al., 2006; Labus and Puttlitz, 2016). A first analysis of the energy functions and calibration of material parameters was carried out for experimental data of uniaxial tensile tests for animal (ovine) white matter with FA = 1 (in the absence of DTI information) (Labus and Puttlitz, 2016). In the experimental data used for white matter, only one loading rate was used. Consequently, as any rate-dependent calibration would be meaningless (and non unique), the

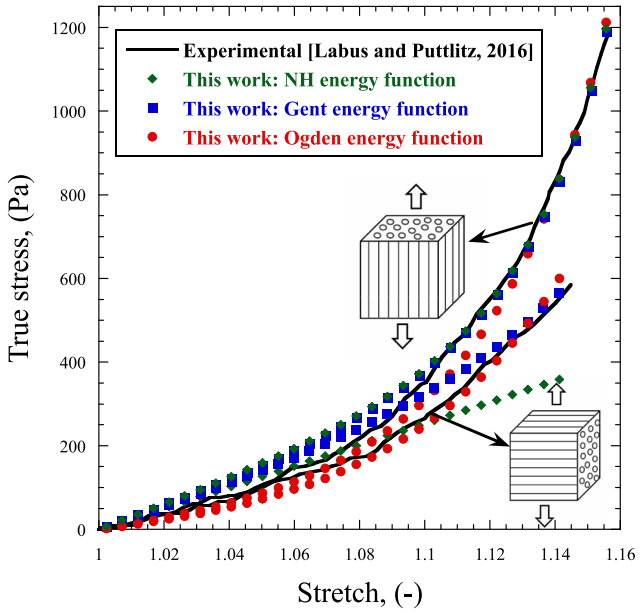

Fig. 4. Stress-stretch experimental curves of ovine white matter in transverse and axon directions (Labus and Puttlitz, 2016) versus models predictions for the three energy functions.

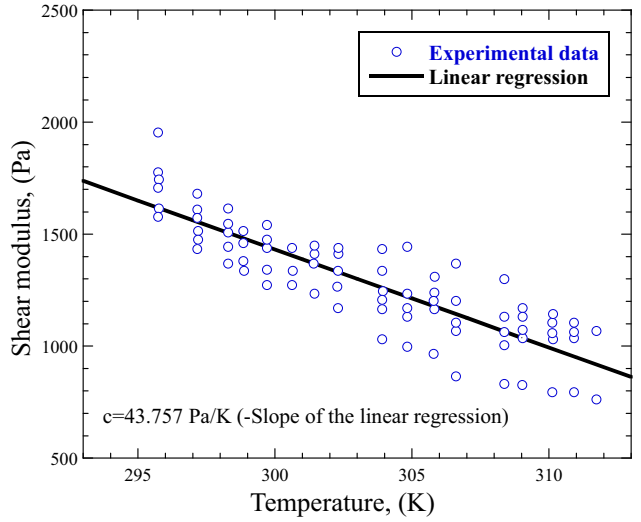

Fig. 5. Experimental data for ovine brain tissue (Liu et al., 2016) and linear regression to determine the temperature-sensitivity parameter c of the model (slope of the linear regression).

viscous branch was not considered here for both the ovine and human models. The loading is applied in both axonal and transverse directions and a comparison between the model predictions and experimental data is shown in Fig. 4. While a good agreement was found for the three energy functions for the tensile tests in the axonal direction, the Neo-Hookean energy function is not able to capture the nonlinear behaviour in the transverse direction (see Table 1). Moreover, although both Gent and Ogden strain energy functions faithfully capture the mechanical behaviour of white matter, the Ogden energy function provides a slightly better fit with a coefficient of determination $R^2 = 0.9934$.

The recent study carried out by Liu et al. (2016) also exhibited a temperature dependence of the brain mechanical properties. In the proposed model, the apparent shear modulus of the white matter (overall response of glial matrix and axons) depends on the temperature through Eqs. (16) and (21). A linear regression with the experiments provided by Liu et al. (2016) was computed to provide the temperature-sensitivity parameter c (slope of the linear regression) over a temperature range from 293 K to 313 K, see Fig. 5.

Human white matter: fractional anisotropy dependent properties. Recent studies have confirmed that the mechanical behaviour of human brain tissue is region dependent (Giordano and Kleiven, 2014; Budday et al., 2017). This means that the

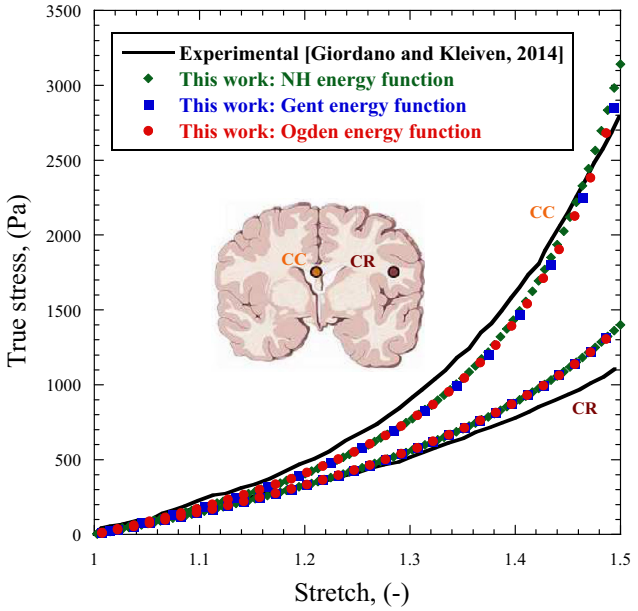

Fig. 6. True stress-stretch experimental curves of different human white matter regions in the mean axonal direction (Giordano and Kleiven, 2014) versus models predictions for the three energy functions (FA = 0.8 for corpus callosum; FA = 0.5 for corona radiata).

stress–strain response of the brain depends on the local microstructure of the tissue, and thus, the FA ranges from 0 to 1 depending on the axonal dispersion. Several works have demonstrated that regions with higher FA exhibit a stiffer response (Velardi et al., 2006; Johnson et al., 2013; Giordano and Kleiven, 2014). In this regard, the corpus callosum –the region that connects the two hemispheres of the brain with a quasi-uniaxial orientation of axons– presents the highest FA (0.6–1.0) with a mean value of 0.8. The other regions of white matter present lower FA, such as the corona radiata (0.4–0.6) with a mean value of 0.5. Focussing on these two regions, Giordano and Kleiven (2014) have proposed a model similar to ours and calibrated its parameters against experimental tests on the human brain (Giordano and Kleiven, 2014).

The analysis of the human white matter is then focussed on the region-dependent mechanical response of the tissue while limiting the loading to the mean axonal direction in all cases. This particular dependence is included in the model through the FA correlation within the different white matter regions. Experimental data of uni-axial tensile tests for human specimens taken from corpus callosum and corona radiata (Giordano and Kleiven, 2014) are compared in Fig. 6 with their corresponding model predictions for the three energy functions (FA = 0.8 for corpus callosum and FA = 0.5 for corona radiata). These model predictions show a good agreement with experiments despite a certain discrepancy in hardening behaviour of corona radiata for large stretches. Since the models were solely calibrated against axonal direction tensile tests, the energy function describing the contribution of the fibres plays a dominant role and the three energy functions considered for the matrix contribution show a similar fit (a complementary calibration against transverse tensile tests would probably have separated them more). As for the animal white matter, the Ogden energy function best fits the experimental results with an average coefficient of determination $\bar{R}^2 = 0.9469$.

The results show a softer mechanical response than that reported by Labus and Puttlitz (2016) for ovine brain. By first identifying the region independent values of k_1 and k_2 for the overall region independent white matter, the model proposed herein can account for the difference between both regions through the FA difference. It must be noted that a recent study carried out by Budday et al. (2017) has shown a stiffer response in the zones with lower values for FA. This discrepancy could be explained by a region dependent stiffness of the glial matrix not accounted for in our model. In this regard, more experimental tests should be conducted in order to clarify this question.

Finally, unlike the other models previously proposed (Wright et al., 2013; Giordano and Kleiven, 2014), the model proposed herein not only accounts for region dependent behaviour associated with axon orientation and dispersion, but it is doing so by coupling it with matrix contributions within a thermodynamically consistent framework able to additionally account for temperature and strain rate dependencies. Such considerations are paramount when considering very high rate deformations and will be explored in a future work.

5.2.2. Skin

The dependence of the mechanical behaviour of skin on applied loading direction (axial and transverse), strain rate and temperature are integrated in the proposed framework. In this section, we focus our discussion on the effects of collagen fibres orientation, strain rate and temperature dependencies.

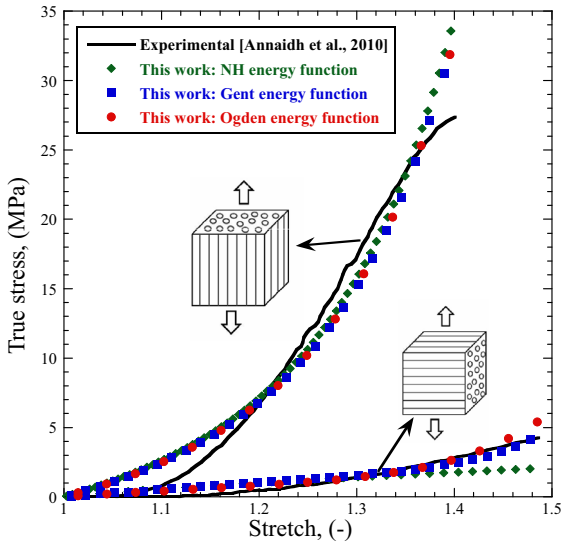

Fig. 7. True stress-stretch experimental curves of human skin in transverse and axon directions (Annaidh et al., 2010) versus model predictions for the three energy functions.

Human skin: fibres orientation dependent properties. The natural orientation of collagen fibres within the dermis leading to the tissue transverse isotropic mechanical behaviour is determined by Langer's lines. These are topological lines that go through the human skin. The work of Annaidh et al. (2010) on human skin was used to study the anisotropy induced by the orientation of the collagen fibres within the tissue. In this study, Annaidh et al. (2010) analysed the influence of this orientation on the mechanical behaviour of skin by carrying out uniaxial tensile tests using specimens excised from the back of seven human cadavers and varying the loading direction.

The model predictions for the different energy functions are compared with the corresponding experimental data for tensile tests in Fig. 7, showing a good correlation between them for both longitudinal and transverse loading conditions. A significant influence of the orientation of collagen fibres was observed. As occurred with white matter, a similar fit was found for all energy functions in the fibres direction due to their predominant contribution in such conditions. Moreover, the Neo-Hookean function failed again to capture the nonlinear behaviour of the transverse direction (see Table 2). The best correlation was also found for the Ogden energy function (Table 2). However, none of the energy functions could capture the toe region of the stress–strain curves in the longitudinal direction.

Animal skin: strain rate and temperature dependent properties. With the aim of illustrating the ability of the model to account for strain rate and temperature dependencies, the work carried out by Zhou et al. (2010) on pig skin was used. In this work, the authors conducted uni-axial tensile tests using pig belly skin at different strain rates and testing temperatures. The tensile tests showed a stress-stretch behaviour defined by a three-stage strain hardening related to the fibres reorientation during the deformation process: a low stiffness region at low stretches; a transition region at medium stretches; and a high stiffness region at large stretches.

Because of the absence of information about the fibres directions within the experimental samples (Zhou et al., 2010), the model predictions were conducted herein assuming full fibres dispersion. This assumption was implemented by defining the structure tensor, according to Eq. (23), as $\hat{\mathbf{A}}_{\mathbf{o}} = \xi \mathbf{I}$ with $\xi = 1/3$. For the different energy functions, the apparent shear modulus (μ for Neo-Hookean and Gent; $\mu\alpha/2$ for Ogden) and the fibre parameter k_1 are of the same order, indicating consistency in the identification process of the model parameters. In addition, to be consistent with the human case, the ratio *apparent shear modulus*/k_1 was retained in the same order of magnitude for the animal skin. The model predictions for the three energy functions are compared against experimental tensile tests in Fig. 8. Gent and Ogden energy functions satisfactorily represent the experimental data in terms of stress-stretch shape, strain rate and temperature dependencies. However, the Neo-Hookean model is not able to capture the mechanical behaviour depending on variations in strain rate and temperature. The best fit was found for Gent and Ogden energy functions with a slightly better prediction of the Gent energy function.

The results confirm the ability of the proposed model to predict the hardening increase with increased loading rate, as observed from experiments with loading rates ranging from 0.25 s^{-1} to 1 s^{-1}. Moreover, the model also provides good predictions when varying testing temperature for hyperthermic temperatures. In this regard, a softening response of the tissue is observed with higher temperatures.

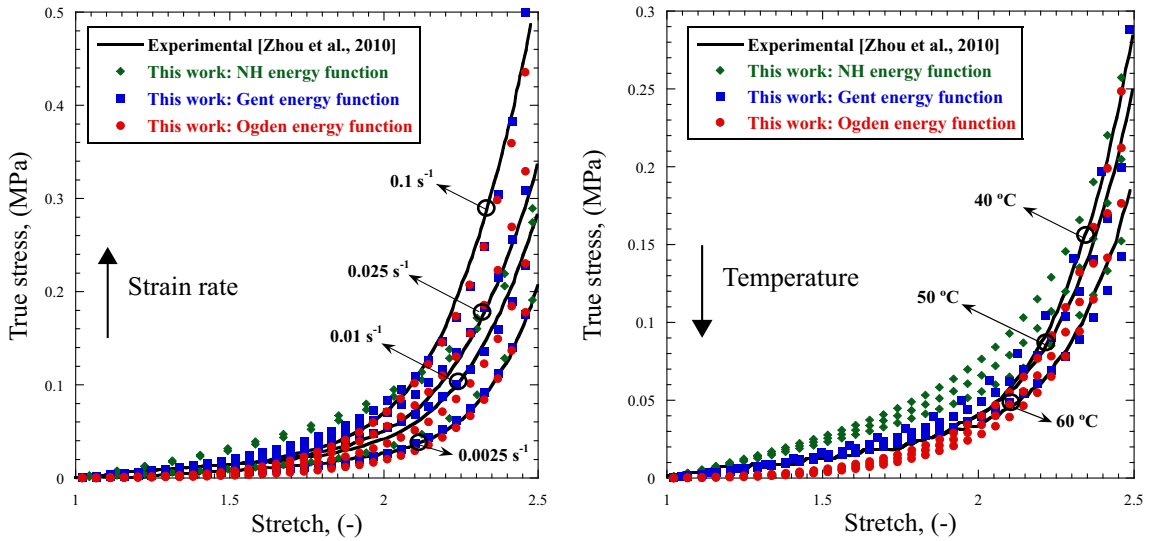

Fig. 8. True stress-stretch experimental curves of pig skin (Zhou et al., 2010) versus model predictions for the three energy functions at: (left) different strain rates (0.0025 s^{-1}, 0.01 s^{-1}, 0.025 s^{-1}, 0.1 s^{-1}) at $T=45$ °C; (right) different temperature (40 °C, 50 °C, 60 °C) at strain rate of 0.1 s^{-1}.

6. Conclusions

The main contribution of this work is the development of a thermodynamically consistent continuum framework for transversely isotropic soft tissues. This framework accounts for transversely isotropy together with strain rate and temperature dependencies. The proposed formulation is based on a Helmholtz free energy function decoupled into the contributions of a viscous-hyperelastic matrix and of the transverse isotropy of fibres.

The constitutive framework was particularised for two transversely isotropic soft tissues in order to illustrate its versatility. The main outcomes of the present work are the following:

- A constitutive model was proposed for white matter. This model takes into account axonal orientation dependent as well as region dependent properties by calibrating two anisotropic parameters for the entire white matter and by making use of the direct value of the FA extracted from DTI measurements for region specialisation. Additionally, our formulation accounts for temperature and, potentially, strain rate dependencies in a consistent manner. This constitutive model was applied to the modelling of animal and human white matters and the results exhibited a good agreement between numerical predictions and experimental data.
- A constitutive model was proposed for skin. This model takes into account strain rate and temperature dependencies, as well as the transverse isotropy arising from the fibre orientation. This constitutive model was applied to the modelling of animal and human skins and the results exhibited a good agreement between numerical predictions and experimental data.
- A methodology for the particularisation of the general constitutive framework was developed. This methodology allows for the adequate identification of the corresponding model parameters depending on the specific soft tissue and the potential energy functions considered. In this work, three different energy functions (Neo-Hookean, Gent and Ogden) were studied for each soft tissue and compared in terms of prediction accuracy of the mechanical behaviour of such soft tissues.

Acknowledgements

The researchers are indebted to the Ministerio de Economía y Competitividad de España (Projects DPI2014-57989-P and DPI2017-85970-R) for the financial support which permitted to conduct part of this work.

D.G.-G. and A.J. acknowledge funding from the European Union's Seventh Framework Programme (FP7 2007-2013) ERC Grant Agreement No. 306587.

Appendix A. Material parameters for the different energy functions applied to each soft tissue

This appendix provides the tables that summarise the material parameters of the different energy functions and the different soft tissues analysed in this work. The model predictions carried out in this work assume incompressibility for both tissues since the bulk modulus of the materials considered here is much higher than the shear modulus.

A.1. White matter

The material parameters for animal and human white matter are provided in Table A.1 and Table A.2 respectively.

Table A.1
Material parameters for ovine white matter identified from the experiments reported by Labus and Puttlitz (2016) and Liu et al. (2016).

Neo-Hookean	**Glial matrix elastic response**			**Axonal response**		
	μ_0 (Pa)	θ_{ref} (K)	c (kPa/K)	k_1 (Pa)	k_2	
	1261	298	−43.757	171.64	18.244	
	Glial matrix viscous response					
	μ_v (Pa)	$\dot{\gamma}_o^v$ (s^{-1})	n	σ_{VT} (Pa)		
	-	-	-	-		
Gent	**Glial matrix elastic response**				**Axonal response**	
	μ_0 (Pa)	j_m	θ_{ref} (K)	c (kPa/K)	k_1 (Pa)	k_2
	1350	0.17	298	−43.757	55	24
	Glial matrix viscous response					
	μ_v (Pa)	j_v	$\dot{\gamma}_o^v$ (s^{-1})	n	σ_{VT} (Pa)	
	-	-	-	-	-	
Ogden	**Glial matrix elastic response**				**Axonal response**	
	μ_0 (Pa)	α	θ_{ref} (K)	c (kPa/K)	k_1 (Pa)	k_2
	500	23	298	−43.757	72	20
	Glial matrix viscous response					
	μ_v (Pa)	β	$\dot{\gamma}_o^v$ (s^{-1})	n	σ_{VT} (Pa)	
	-	-	-	-	-	

Table A.2
Material parameters for human white matter identified from the experiments reported by Giordano and Kleiven (2014). Temperature dependence is not considered.

Neo-Hookean	**Glial matrix elastic response**			**Axonal response**		
	μ_0 (Pa)	θ_{ref} (K)	c (Pa/K)	k_1 (Pa)	k_2	
	580.046	-	-	258.982	1.805	
	Glial matrix viscous response					
	μ_v (Pa)	$\dot{\gamma}_o^v$ (s^{-1})	n	σ_{VT} (Pa)		
	-	-	-	-		
Gent	**Glial matrix elastic response**	**e**			**Axonal response**	
	μ_0 (Pa)	j_m	θ_{ref} (K)	c (Pa/K)	k_1 (Pa)	k_2
	580.045	84.57	-	-	257.973	1.798
	Glial matrix viscous response					
	μ_v (Pa)	j_v	$\dot{\gamma}_o^v$ (s^{-1})	n	σ_{VT} (Pa)	
	-	-	-	-	-	
Ogden	**Glial matrix elastic response**				**Axonal response**	
	μ_0 (Pa)	α	θ_{ref} (K)	c (Pa/K)	k_1 (Pa)	k_2
	583.5	1.934	-	-	264.586	1.692
	Glial matrix viscous response					
	μ_v (Pa)	β	$\dot{\gamma}_o^v$ (s^{-1})	n	σ_{VT} (Pa)	
	-	-	-	-	-	

A.2. Skin

The material parameters for human and animal skin are provided in Table A.3 and Table A.4 respectively.

Table A.3
Material parameters for human skin identified from the experiments reported by Annaidh et al. (2010).

Neo-Hookean	**Ground substance elastic response**			**Collagen response**		
	μ_0 (kPa)	θ_{ref} (K)	c (Pa/K)	k_1 (MPa)	k_2	
	927	-	-	6.925	0.72	
	Ground substance viscous response					
	μ_v (kPa)	$\dot{\gamma}_o^v$ (s^{-1})	n	σ_{VT} (MPa)		
	-	-	-	-		
Gent	**Ground substance elastic response**				**Collagen response**	
	μ_0 (kPa)	j_m	θ_{ref} (K)	c (Pa/K)	k_1 (MPa)	k_2
	845	0.738	-	-	6.656	0.696
	Ground substance viscous response					
	μ_v (kPa)	j_v	$\dot{\gamma}_o^v$ (s^{-1})	n	σ_{VT} (MPa)	
	-	-	-	-	-	
Ogden	**Ground substance elastic response**				**Collagen response**	
	μ_0 (kPa)	α	θ_{ref} (K)	c (Pa/K)	k_1 (MPa)	k_2
	98.44	15.815	-	-	6.971	0.633
	Ground substance viscous response					
	μ_v (kPa)	β	$\dot{\gamma}_o^v$ (s^{-1})	n	σ_{VT} (MPa)	
	-	-	-	-	-	

Table A.4
Material parameters for pig skin identified from the experiments reported by Zhou et al. (2010).

Neo-Hookean	**Ground substance elastic response**			**Collagen response**		
	μ_0 (kPa)	θ_{ref} (K)	c (Pa/K)	k_1 (kPa)	k_2	
	1	318	$-1.3\cdot10^{-4}$	4.22	0.65	
	Ground substance viscous response					
	μ_v (kPa)	$\dot{\gamma}_o^v$ (s^{-1})	n	σ_{VT} (MPa)		
	27	0.0025	0.02	2000		
Gent	**Ground substance elastic response**				**Collagen response**	
	μ_0 (kPa)	j_m	θ_{ref} (K)	c (Pa/K)	k_1 (kPa)	k_2
	1	15.098	318	$-9.8\cdot10^{-5}$	3.2	0.825
	Ground substance viscous response					
	μ_v (kPa)	j_v	$\dot{\gamma}_o^v$ (s^{-1})	n	σ_{VT} (MPa)	
	14	4.255	0.0025	0.019	2000	
Ogden	**Ground substance elastic response**				**Collagen response**	
	μ_0 (kPa)	α	θ_{ref} (K)	c (Pa/K)	k_1 (kPa)	k_2
	0.35	5.115	318	$-3.4\cdot10^{-5}$	2.13	1.062
	Ground substance viscous response					
	μ_v (kPa)	β	$\dot{\gamma}_o^v$ (s^{-1})	n	σ_{VT} (MPa)	
	1.1	8.31	0.0025	0.025	2000	

References

Advani, S.G., Tucker III, C.L., 1987. The use of tensors to describe and predict fiber orientation in short fiber composites. J. Rheol. 31 (8), 751–784.

Annaidh, A.N., Ottenio, M., Bruyère, K., Destrade, M., Gilchrist, M.D., 2010. Mechanical properties of excised human skin. In: Lim, C.T., Goh, J.C.H. (Eds.), Proceedings of the 6th World Congress of Biomechanics (WCB 2010). (August 1-6, 2010 IFMBE Singapore), 31. Springer, Berlin, Heidelberg.

Arroyave, G.,A.I., Lima, R.G., Martins, P.A.L.S., Ramião, N., Jorge, R.M.N., 2015. Methodology for mechanical characterization of soft biological tissues: arteries. In: 4th International Conference on Tissue Engineering Procedia Engineer., (ITE 2015), 110, pp. 74–81.

Bergström, J., 2015. Mechanics of Solid Polymers: Theory and Computational Modeling, First ed. William Andrew, San Diego, USA.

Budday, S., Sommer, G., Birkl, C., Langkammer, C., Haybaeck, J., Kohnert, J., Bauer, M., Paulsen, F., Steinmann, P., Kuhl, E., Holzapfel, G.A., 2017. Mechanical characterization of human brain tissue. Acta Biomater 48, 319–340.

Carniel, T.A., Fancello, E.A., 2017. A transversely isotropic coupled hyperelastic model for the mechanical behavior of tendons. J. Biomech. 54, 49–57.

Cercignani, M., Inglese, M., Pagani, E., Comi, G., Filippi, M., 2001. Mean diffusivity and fractional anisotropy histograms of patients with multiple sclerosis. Am. J. Neuroradiol. 22, 952–958.

Chatelin, S., Deck, C., Willinger, R., 2012. An anisotropic viscous hyperelastic constitutive law for brain material finite-element modeling. Biorheology 27, 26–37.

Clemmer, J., Liao, J., Davis, D., Horstemeyer, M.F., Williams, L.N., 2010. A mechanistic study for strain rate sensitivity of rabbit patellar tendon. J. Biomech. 43, 2785–2791.

Coleman, B.D., Gurtin, M.E., 1967. Thermodynamics with internal state variables. The J. Chem. Phys. 45, 597–613.

Coleman, B.D., Noll, W., 1963. The thermodynamics of elastic materials with heat conduction and viscosity. Arch. Rational. Mech. Anal. 13, 167–178.

Cowin, S.C., Humphrey, J.D., 2001. Cardiovascular Soft Tissue Mechanics. Springer.

Feng, Y., Okamoto, R.J., Namani, R., Genin, G.M., Bayly, P., 2013. Measurements of mechanical anisotropy in brain tissue and implications for transversely isotropic material models of white matter. J. Mech. Behav. Biomed. Mater. 23, 117–132.

Fung, Y.C., 1981. Biomechanics: Mechanical Properties of Living Tissues. Springer.

Garcia-Gonzalez, D., Zaera, R., Arias, A., 2017a. A hyperelastic-thermoviscoplastic constitutive model for semi-crystalline polymers: application to PEEK under dynamic loading conditions. Int. J. Plast. 88, 27–52.

Garcia-Gonzalez, D., Jayamohan, J., Sotiropoulos, S.N., Yoon, S.-H., Cook, J., Siviour, C.R., Arias, A., Jérusalem, A., 2017b. On the mechanical behaviour of PEEK and HA cranial implants under impact loading. J. Mech. Behav. Biomed. Mater. 69, 342–354.

Gasser, T.C., Ogden, R.W., Holzapfel, G.A., 2006. Hyperelastic modelling of arterial layers with distributed collagen fibre orientations. J. R. Soc. Interface 3, 15–35.

Gent, A.N., 1996. A new constitutive relation for rubber. Rubber Chem. Technol. 69 (1), 59–61.

Giordano, C., Kleiven, S., 2014. Connecting fractional anisotropy from medical images with mechanical anisotropy of a hyperviscoelastic fibre-reinforced constitutive model for brain tissue. J. R. Soc. Interface 1, 20130914.

Goriely, A., Geers, M.G.D., Holzapfel, G.A., Jayamohan, J., Jérusalem, A., Sivaloganathan, S., Squier, W., van Dommelen, J.A.W., Waters, S., Kuhl, E., 2015. Mechanics of the brain: perspectives, challenges, and opportunities. Biomech. Model. Mechanobiol. 14, 931–965.

Guo, Z., Peng, X., Moran, B., 2007. Mechanical response of neo-Hookean fiber reinforced incompressible nonlinearly elastic solids. Int. J. Solids Struct. 44, 1949–1969.

Holzapfel, G.A., Gasser, T.C., Ogden, R.W., 2000. A new constitutive framework for arterial wall mechanics and a comparative study of material models. J. Elast. 61, 1–48.

Humphrey, J.D., Strumpf, R.K., Yin, F.C.P., 1990. Determination of a constitutive relation for passive myocardium. J. Biomech. Eng-T ASME 112, 333–346.

Johnson, C.L., McGarry, M.D.J., Gharibans, A.A., Weaver, J.B., Paulsen, K.D., Wang, H., Olivero, W.C., Sutton, B.P., Georgiadis, J.G., 2013. Local mechanical properties of white matter structures in the human brain. Neuroimage 79, 145–152.

Kulkarni, S.G., Gao, X-L., Horner, S.E., Mortlock, R.F., Zheng, J.Q., 2016. A transversely isotropic visco-hyperelastic constitutive model for soft tissues. Math. Mech. Solids 21, 747–770.

Labus, K.M., Puttlitz, C.M., 2016. An anisotropic hyperelastic constitutive model of brain white matter in biaxial tension and structural–mechanical relationships. J. Mech. Behav. Biomed. 62, 195–208.

Li, K., Ogden, R.W., Holzapfel, G.A., 2017. Modeling fibrous tissues with a general invariant that excludes compressed fibers. J. Mech. Phys. Solids 110, 38–53.

Limbert, G., Middleton, J., 2004. A transversely isotropic viscohyperelastic material application to the modeling of biological soft connective tissues. Int. J. Solids Struct. 41, 4237–4260.

Liu, Y-L., Lia, G-Y., He, P., Mao, Z-Q., Cao, Y., 2016. Temperature-dependent elastic properties of brain tissues measured with the shear wave elastography method. J. Mech. Behav. Biomed. 65, 652–656.

Maurel, W., Wu, Y., Magnenat Thalmann, N., Thalmann, D., 1997. Biomechanical Models for Soft Tissue Simulation. Springer, New York.

Meaney, D.F., 2003. Relationship between structural modeling and hyperelastic material behavior: application to CNS white matter. Biomech. Model Mechanbiol. 1, 279–293.

Mohammadkhah, M., Murphy, P., Simms, C.K., 2016. The in vivo passive elastic response of chicken pectoralis muscle to applied tensile and compressive deformation. J. Mech. Behav. Biomed. 62, 468–480.
Murphy, J.G., 2013. Transversely isotropic biological, soft tissue must be modelled using both anisotropic invariants. Eur. J. Mech. A-Solid. 42, 90–96.
Natali, A.N., Pavan, P.G., Carniel, E.L., Lucisano, M.E., Taglialavoro, G., 2005. Anisotropic elasto-damage cosntitutive model for the biomechanical analysis of tendons. Med. Eng. Phys. 27, 209–214.
Ng, B.H., Chou, S.M., Lim, B.H., Chong, A., 2004. Strain rate effect on the failure properties of tendons. Proc. Inst. Mech. Eng. H. 218 (3), 203–206.
Ning, X., Zhu, Q., Lanir, Y., Margulies, S.S., 2006. A transversely isotropic viscoelastic constitutive equation for brainstem undergoing finite deformation. J. Biomech. Eng. 128, 925–933.
Ogden, R.W., 1972. Large deformation isotropic elasticity – on the correlation of theory and experiment for incompressible rubberlike solids. Proc. R. Soc. Lond. Ser. A, Math. Phys. Sci. 326, 565–584.
Ogden, R.W., Saccomandi, G., Sgura, I., 2004. Fitting hyperelastic models to experimental data. Comput. Mech. 34, 484–502.
Pervin, F., Chen, W.W., 2009. Dynamic mechanical response of bovine gray matter and white matter brain tissues under compression. J. Biomech. 42, 731–735.
Pierpaoli, C., Basser, P.J., 1996. Toward a quantitative assessment of diffusion anisotropy. Magn. Reson. Med. 36 (6), 893–906.
Pietsch, R., Wheatley, B.B., Haut Donahue, T.L., Gilbrech, R., Prabhu, R., Liao, J., Williams, L.N., 2014. Anisotropic compressive properties of passive porcine muscle tissue. J. Biomech. Eng. 136 (11). doi:10.1115/1.4028088.
Prange, M.T., Margulies, S.S., 2002. Regional, directional, and age dependent properties of the brain undergoing large deformation. J. Biomech. Eng. 124, 244–252.
Rivlin, R.S., 1948. Large elastic deformations isotropic materials. IV. Further developments of the general theory. Philos. Trans. R. Soc. A 241 (835), 379–397.
Valero, C., Javierre, E., García-Aznar, J.M., Gómez-Benito, M.J., Menzel, A., 2015. Modeling of anisotropic wound healing. J. Mech. Phys. Solids 79, 80–91.
Velardi, F., Fraternali, F., Angelillo, M., 2006. Anisotropic constitutive equations and experimental tensile behavior of brain tissue. Biomech. Model. Mech. 5, 53–61.
Wang, N., Liu, W., Huang, J., Ma, K., 2014. The structure–mechanical relationship of palm vascular tissue. J. Mech. Behav. Biomed. 36, 1–11.
Wright, R.M., Post, A., Hoshizaki, B., Ramesh, K.T., 2013. A multiscale computational approach to estimating axonal damage under inertial loading of the head. J. Neurotraum. 30, 102–118.
Zhou, B., Xu, F., Chen, C.Q., Lu, T.J., 2010. Strain rate sensitivity of skin tissue under thermomechanical loading. Philos. Trans. R. Soc. A 368, 679–690.
Zulliger, M.A., Fridez, P., Hayashi, K., Stergiopulos, N., 2004. A strain energy function for arteries accounting for wall composition and structure. J. Biomech. 37, 989–1000.